Energy 288 (2024) 129801

Contents lists available at ScienceDirect

Energy

journal homepage: www.elsevier.com/locate/energy

# A novel integrated SOC–SOH estimation framework for whole-life-cycle lithium-ion batteries

Haichi Huang [a,b,c,d], Chong Bian [e], Mengdan Wu [f], Dong An [a,b,c,d,*], Shunkun Yang [f]

[a] National Innovation Center for Digital Fishery, China Agricultural University, Beijing, 100083, China
[b] Key Laboratory of Smart Farming Technologies for Aquatic Animals and Livestock, Ministry of Agriculture and Rural Affairs, China Agricultural University, Beijing, 100083, China
[c] Beijing Engineering and Technology Research Center for Internet of Things in Agriculture, China Agricultural University, Beijing, 100083, China
[d] College of Information and Electrical Engineering, China Agricultural University, Beijing, 100083, China
[e] Center of Artificial Intelligence and Intelligent Operation Research and Development, China Mobile Research Institute, Beijing, 100053, China
[f] School of Reliability and Systems Engineering, Beihang University, Beijing, 100191, China

ARTICLE INFO

*Keywords:*
State of health
State of charge
Lithium-ion battery
Gated recurrent unit
Temporal convolutional network

ABSTRACT

Accurate estimating the state of health (SOH) and state of charge (SOC) is crucial for ensuring the reliable and safe operation of lithium-ion batteries. Traditional methods for the joint estimation of SOC and SOH typically rely on separate models, resulting in a decoupling of their relationship. Moreover, the current convolutional and recurrent-based deep models overlook the inherent connection between local features and global temporal features. These limitations not only hinder the extraction of combined feature information relevant to SOC and SOH during the charging process, but also increase computational complexity and diminish estimation accuracy. To solve these problems, this study proposes a novel SOC–SOH Estimation Framework (SSEF). The framework achieves parameter sharing by segmented training, effectively accounting for the intrinsic coupling between SOC and SOH. This enables a unified joint estimation of the two variables, leading to a substantial enhancement in efficiency. Additionally, a novel charging encoder that alternates between Temporal Convolutional Network and Bidirectional Gated Recurrent Unit is designed. It captures local temporal information and long-term dependencies related to SOC and SOH during charging. SSEF enables precise SOC and SOH estimation for whole-life-cycle lithium-ion batteries, enhancing accuracy and efficiency compared to prevalent methods.

## 1. Introduction

Lithium-ion battery (LiB) is widely considered as a promising power source for electric vehicles, owing to their high energy density, long cycle life, and low self-discharge rate. An efficient and accurate battery management system (BMS) is crucial for the effective management of lithium-ion batteries. State of charge (SOC) and state of health (SOH) are two critical indicators used in BMS, providing information about the current charge level and overall health status of the battery. Specifically, SOH is defined as the ratio between the available capacity and the battery's nominal capacity, while SOC is defined as the percentage of remaining capacity relative to the maximum available capacity. Reliable SOC estimation can accurately measure the remaining driving range of the vehicle and balance the battery pack. Accurate SOH estimation not only facilitates correct SOC estimating, but also helps prevent traffic accidents caused by failure to timely replace batteries with severe capacity degradation.

However, the response of the internal chemical reactions and physical processes of the battery to different voltages and currents is nonlinear, making it difficult to accurately control and monitor the SOC and SOH. Moreover, the battery's actual capacity undergoes changes over time, with a gradual decrease in capacity and electrochemical performance after multiple charge and discharge cycles. This presents further obstacles in accurately estimating SOC. In the realm of SOC estimation, traditional methods can be broadly categorized into three main groups: Coulomb counting [1], Open Circuit Voltage (OCV) method [2], and model-based approaches [3]. However, Coulomb counting suffers from long-term cumulative errors, while the OCV method is not well-suited for real-world usage in dynamic electric vehicles due to the requirement of load disconnection. Furthermore, model-based methods can be costly in terms of experiments and heavily reliant on the chosen model structure [4]. Similarly, when it comes to SOH estimation, conventional approaches mainly include direct calculation methods [5]

* Corresponding author at: National Innovation Center for Digital Fishery, China Agricultural University, Beijing, 100083, China.
*E-mail address:* andong@cau.edu.cn (D. An).

https://doi.org/10.1016/j.energy.2023.129801
Received 31 August 2023; Received in revised form 24 October 2023; Accepted 25 November 2023
Available online 28 November 2023

and model-based methods [6,7]. They often necessitate strict hardware conditions [8] or rely extensively on accurately derived model parameters [9], making their application in online scenarios challenging. In recent years, data-driven approaches for SOC and SOH estimation have gained significant popularity. Data-driven methods [10,11] utilize machine learning or deep learning algorithms to discern the nonlinear relationship between battery measurement parameters and SOC or SOH. These approaches do not necessitate precise formulas or model structures, yet they can achieve a high level of accuracy [12].

Deep learning methods have emerged as a crucial subset within the realm of data-driven methods. Early studies explored multi-layer perceptron (MLP) networks for SOC estimation [13], but they struggled to capture temporal information from continuous time series data. To address this, long short-term memory (LSTM) and gated recurrent unit (GRU) networks were introduced, as they can process sequential data and capture long-term dependencies [14–16]. Researchers utilized LSTM models to estimate SOC under various conditions, achieving excellent performance [17]. Bian et al. [18] proposed a stacked bidirectional LSTM (SBLSTM) model that achieves superior accuracy in SOC estimation and is applicable to different types of batteries under various environmental temperature conditions. Based on temporal convolutional network (TCN) and LSTM, Hu et al. [19] proposed a TCN-LSTM model with better performance than TCN or LSTM alone. Similar to SOC estimation, machine learning methods [20–22] and deep learning methods have gained popularity in SOH estimation [23–25]. LSTM with gated units has become a preferred choice for overcoming gradient issues and improving SOH estimation [26,27]. Studies have proposed advanced models, such as attention-based spatial–temporal LSTM (AST-LSTM) by Li et al. [28,29] and CNN–LSTM based on CNN and LSTM by Xu et al. [30], which exhibit outstanding performance in terms of accuracy and error metrics. Furthermore, Ungurean et al. proposed an online SOH estimation algorithm based on GRU, which exhibited superior performance compared to LSTM across different temperature values. Additionally, the integration of domain adaptation layers with LSTM has been employed to enhance the robustness and accuracy of SOH estimation across diverse datasets [31].

The above methods for estimating battery SOH heavily depend on historical capacity variation or complete charging data. However, in real-world applications, accurately obtaining the battery's historical capacity is difficult, and complete discharge data is often unavailable due to incomplete discharges during practical operations. In automotive applications, the constant current–constant voltage (CC–CV) charging protocol is widely adopted due to its relatively stable parameter variations throughout the battery's whole-life-cycle. Taking advantage of this characteristic, researchers have extracted various features from the CC–CV charging process to represent the battery's SOH [32]. Considering the aforementioned factors, Zheng et al. [33] used the CNN-GRU model to complete the estimation of SOH in the random charging part and achieved good results. Deng et al. [34] proposed a novel method for SOH estimation based on random partial charging processes and Sparse Gaussian Process Regression (GPR), which yielded promising results. Qian et al. [35] introduced a one-dimensional CNN (1D-CNN) model for estimating the actual capacity of batteries using random charging curve segments as input, which yielded excellent outcome. The methods utilize the parameter variation information during charging to estimate SOH but fail to consider the information about SOC in the parameter changes.

Although the above methods can effectively estimate SOC or SOH, they are constrained by their single-target nature, limiting them to forecast only one variable. Moreover, precise SOH estimation during CC–CV charging relies exclusively on specific charging data within a predetermined range [34], whereas SOC estimation necessitates an assessment across the entire charging process. Owing to these constraints, the aforementioned data-driven approaches decouple the estimation of SOC and SOH in lithium-ion batteries, treating them as independent variables without considering their interdependencies. One approach to address this is to use the estimated results from the SOH model as the input for the SOC model, employing two independent models for estimation [36]. However, these approaches overlook the latent intrinsic correlations present in SOC and SOH charging data, leading to elevated computational complexity and diminished precision in estimation. Moreover, the current convolutional and recurrent-based deep models have overlooked the intrinsic link between local features and global temporal features. This oversight hampers their ability to effectively capture temporal information during the charging process, ultimately undermining the precision of estimations.

In response to the aforementioned issues, a SOC–SOH estimation framework (SSEF) is proposed, achieving parameter sharing through segmented training. Initially, it conducts joint training on charging data within specific ranges, capturing the shared characteristics of SOC and SOH. Subsequently, some parameters are transitioned to the SOC estimation across the entire charging process. It effectively couples the estimation of SOC and SOH, facilitating the comprehensive extraction of charging-related information and enhancing estimation accuracy. Additionally, a charging encoder that alternates between TCN and GRU is designed. This composite architecture effectively leverages TCN's ability to learn from local temporal regions and GRU's capability to capture long-term dependencies. This fusion empowers the deep extraction of combined local features and comprehensive global information between SOC and SOH during the charging cycle. By thoroughly considering the inherent coupling between SOC and SOH, this framework achieves efficient and accurate estimation of both SOC and SOH using a unified model.

Our contributions of this research are summarized as follows:

1. A segmented training approach is introduced for the combined estimation of SOC and SOH. By sharing parameters, the integration of SOC and SOH information is realized, effectively capturing their interdependent connection. This methodology enables efficient joint estimation.

2. A novel charging encoder, alternating between TCN and GRU, synergizes the local temporal learning of TCN with the long-term dependency capture of GRU. This enhances the extraction of underlying SOC–SOH correlations during charging, significantly boosting estimation accuracy.

3. The accuracy and efficiency of SSEF in estimating SOC and SOH throughout the entire lifespan of various batteries were verified using a dataset from the University of Maryland.

The rest of the paper is organized as follows. Section 2 introduces TCN and GRU. In Section 3, a comprehensive overview is provided for the composition of SSEF, along with the training and online estimation strategies employed. Section 4 presents the dataset and experimental procedures, and concluding remarks are given in Section 5.

## 2. Technical preliminaries

### 2.1. Temporal convolutional network

One-dimensional convolution (1D-CNN) is a fundamental operation in CNN that plays a crucial role in capturing local patterns and extracting features from sequential data. It involves applying a sliding kernel over the input sequence to generate a feature map. The mathematical representation of one-dimensional convolution can be expressed as:

$$y(t) = \sum_{k=1}^{K} x(t-k) \cdot w(k) \tag{1}$$

In the above equation, $y(t)$ denotes the output at time step $t$, $x(t-k)$ represents the input at time step $t-k$, $w(k)$ denotes the kernel weights, and $K$ represents the kernel size. One-dimensional convolution enables parameter sharing and efficient feature extraction from sequential data, making it particularly well-suited for tasks such as time series analysis and natural language processing.

TCN are an extension of CNNs specifically designed to model sequential data with long-range dependencies. TCNs incorporate dilated convolutions and residual connections to effectively capture both local and global patterns in the data. The TCN architecture can be represented as:

$$y(t) = f(x(t), x(t-1), \ldots, x(t-L+1)) \tag{2}$$

Here, $y(t)$ represents the output at time step $t$, $x(t)$ denotes the input at time step $t$, and $L$ represents the receptive field size. The receptive field determines the range of dependencies that can be captured by the TCN. By utilizing dilated convolutions, TCN can effectively model distant dependencies without a significant increase in the number of parameters.

The key advantage of TCN lies in its ability to capture long-range dependencies while maintaining computational efficiency. TCN provides a powerful tool for analyzing sequential data. 1D-CNN allows for local feature extraction, while TCNs extend this concept to capture long-range dependencies. These techniques have proven to be highly effective in various applications and continue to advance the field of sequential data analysis.

### 2.2. Bidirectional gated recurrent units

GRU has emerged as a popular choice for sequence modeling tasks due to its ability to mitigate the vanishing gradient problem encountered by traditional RNN. By incorporating gating mechanisms, GRU effectively controls the flow of information, facilitating better learning of sequential patterns. An extension of GRU, known as BiGRU, consists of two GRU layers: one processes the input sequence in the forward direction, while the other operates in the backward direction. The BiGRU model, by considering information from both directions, enables a comprehensive understanding of the input sequence.

Assumptions, $x_t$ represents the input at time step $t$, and $h_t^f$ and $h_t^b$ denote the hidden states of the forward and backward GRU layers at time step $t$, respectively. The superscripts $f$ and $b$ denote the forward and backward directions. The mathematical formulation of Forward GRU is as follows:

$$z_t^f = \sigma(W_z^f x_t + U_z^f h_{t-1}^f + b_z^f) \tag{3}$$

$$r_t^f = \sigma(W_r^f x_t + U_r^f h_{t-1}^f + b_r^f) \tag{4}$$

$$\tilde{h}_t^f = \tanh(W_h^f x_t + U_h^f (r_t^f \odot h_{t-1}^f) + b_h^f) \tag{5}$$

$$h_t^f = (1 - z_t^f) \odot h_{t-1}^f + z_t^f \odot \tilde{h}_t^f \tag{6}$$

In the forward GRU equations, the update gate $z_t^f$, reset gate $r_t^f$, and candidate hidden state $\tilde{h}_t^f$ are computed based on the input $x_t$ and the previous hidden state $h_{t-1}^f$. The current forward hidden state $h_t^f$ is then determined by blending the previous forward hidden state $h_{t-1}^f$ with the candidate hidden state $\tilde{h}_t^f$ using the update gate $z_t^f$. In contrast, the Backward GRU operates in reverse, capturing dependencies from the future. The mathematical representation of the BiGRU is presented below:

$$h_t^{bi} = [h_t^f, h_t^b] \tag{7}$$

BiGRU is a powerful model for capturing dependencies in sequential data by considering both past and future contexts. The update gate determines the extent to which the previous hidden state should be retained and the candidate hidden state should be incorporated. The reset gate controls the amount of information from the previous hidden state that should be discarded. By leveraging these gates and the candidate hidden state, BiGRU effectively captures relevant information for the current time step, facilitating comprehensive sequence understanding.

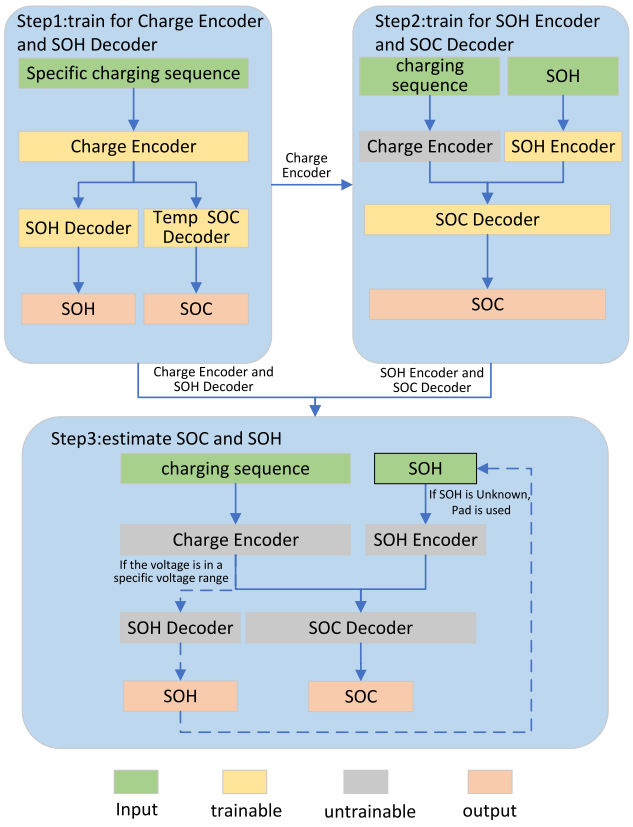


**Fig. 1.** Flowchart of the SOC–SOH estimation process.

## 3. Methodology

### 3.1. SOC-SOH estimation framework

The SSEF framework comprises four main components: Charge Encoder, SOH Encoder, SOC Decoder, and SOH Decoder. The Charge Encoder captures the information regarding parameter variations during the charging process and is composed of 1D-CNN, TCNGRU, and Dense Layer modules. The SOH Encoder, SOC Decoder, and SOH Decoder are responsible for encoding the current SOH information, decoding the SOC values, and decoding the SOH values, respectively. All of these components utilize Dense Layer.

As shown in Fig. 1, the application of the SSEF can be broken down into three steps. In step 1, training is initiated by utilizing data from a specific range of charging voltage, leading to the acquisition of the charge encoder and SOH decoder. In Step 2, the previously obtained charging encoder is employed as pre-trained parameters, facilitating the training of the SOH encoder and SOC decoder with comprehensive charging data. This equips the model with the capability to accurately estimate SOC throughout the entire battery charging process. Finally, in Step 3, amalgamating the charging encoder and SOH decoder from the first step with the SOH encoder and SOC decoder from the second step results in a comprehensive estimation model for both SOC and SOH. SSEF is a novel framework for whole-life-cycle lithium-ion batteries, offering several advantages over current models. Detailed explanations of these using processes will be provided in the subsequent sections.

### 3.2. Charge encoder and SOH decoder

In order to achieve better estimation of SOC throughout the battery's whole-life-cycle, it is necessary to obtain the current battery's SOH. And, it is important to note that accurate estimation of SOH

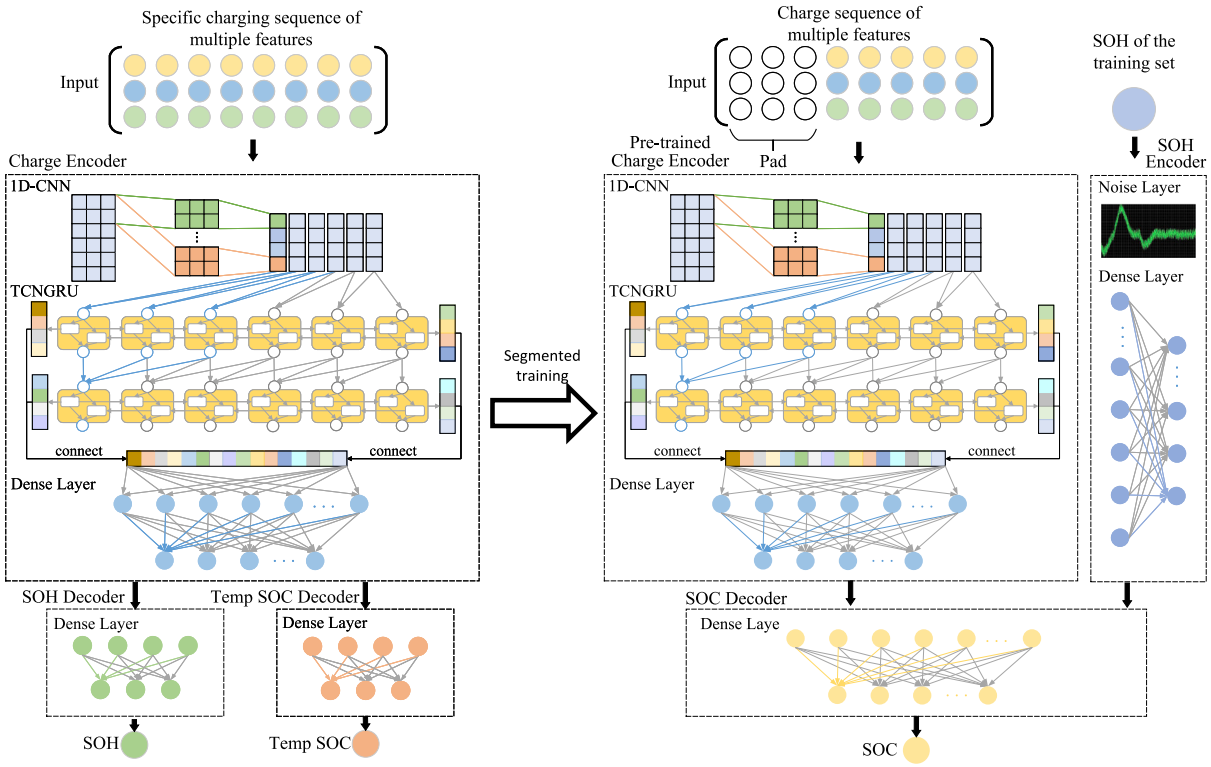


**Fig. 2.** Structure of the proposed SSEF.

requires data collected within a specific voltage range during the charging process. Therefore, our initial focus is on training a joint estimation model for SOC and SOH using multiple data points within the designated voltage range of each charging cycle. The goal is to obtain a Charge Encoder that has learned the features of SOC and SOH, as well as an SOH Decoder capable of estimation the SOH. Fig. 2 (left) provides an illustration of the overall model structure for this step. As the battery evolves over time, multiple observed variables emerge at each time point. By arranging these variables in temporal order, a sequence of features is formed. This sequence is fed as input to the model's Charge Encoder, which consists of a one-dimensional convolutional layer(1D-CNN), TCN layer, BiGRU layer, and a Dense layer.

The first layer of the encoder consists of a 1D-CNN, which serves two primary purposes: dimension transformation and local feature extraction. It plays a crucial role in capturing significant patterns and local structures within the input sequence. Following the 1D-CNN, the core module of the encoder is composed of a sequence of TCN and BiGRU layers, organized in the TCN-BiGRU-TCN-BiGRU fashion. With the increasing number of layers, the convolutional receptive field progressively expands. The alternating utilization of TCN and BiGRU facilitates the extraction of both local temporal information and global temporal information. Finally, the final hidden state from the last time step of each BiGRU layer is concatenated and passed to a fully connected layer to accomplish the final encoding task.

To facilitate accurate estimation of SOH and enable the decoders to effectively learn the sequential characteristics of both SOC and SOH, two distinct decoders are employed following the encoder. These decoders consist of two Dense layers each, with the final layer producing a 1-dimensional output. It is important to note that the SOH decoder will be utilized in subsequent estimation tasks, while the SOC decoder is temporary and solely utilized in this particular step. To enhance the joint estimation performance, a customized loss function tailored specifically for the joint estimation task has been devised:

$$\text{Loss} = \alpha \frac{1}{N} \sum_{i=1}^{N} (y_{\text{SOC}}^{(i)} - \hat{y}_{\text{SOC}}^{(i)})^2 + \beta \frac{1}{N} \sum_{i=1}^{N} (y_{\text{SOH}}^{(i)} - \hat{y}_{\text{SOH}}^{(i)})^2 \tag{8}$$

The variables $y_{SOC}^{(i)}$ and $\hat{y}_{SOC}$ correspond to the true and estimated SOC values, respectively, for the $i$th sequence estimation. Similarly, $y_{SOH}^{(i)}$ and $\hat{y}_{SOH}$ represent the true and estimated SOH values, respectively, for the $i$th sequence estimation. The parameters $\alpha$ and $\beta$ are two crucial hyperparameters in the first step of training. Their role is to balance the loss, thereby optimizing the Charge Encoder and SOH Decoder more effectively. As the subsequent training phase is specifically directed at the SOC Decoder, with no further training for the SOH Decoder, it is recommended to set the value of $\beta$ slightly greater than $\alpha$. However, the gap should not be too large to ensure that the Charge Encoder can effectively learn valid information related to SOC.

### 3.3. SOH encoder and SOC decoder

In the preceding steps, we have obtained a Charge Encoder that captures both SOC and SOH features from the sequence data of the charging process. In this phase, we focus on training the SOC estimation. As depicted in Fig. 2(right), we employ the pre-trained Charge Encoder to encode the sequence data of the charging process while incorporating a dedicated SOH Encoder designed specifically for encoding SOH. Subsequently, both encoded representations are simultaneously inputted to the SOC decoder, enabling accurate decoding and estimation of SOC. The SOH Encoder consists of a Gaussian noise layer and a fully connected layer. It is worth noting that the input SOH during the actual estimation represents a estimated value that may have some inherent error, which differs from the measured SOH values used in the training process. To alleviate overfitting, we intentionally introduce Gaussian noise to the input SOH during the training process. As for the SOC decoder, it consists of two fully connected layers, with the final layer having a 1-dimensional output, responsible for estimation the SOC value.

Based on practical usage requirements, it is necessary to estimate the SOC for the entire charging process of the whole-life-cycle. However, the initial stage of CC charging does not provide a sufficiently long sequence to be effectively inputted into the model. To overcome

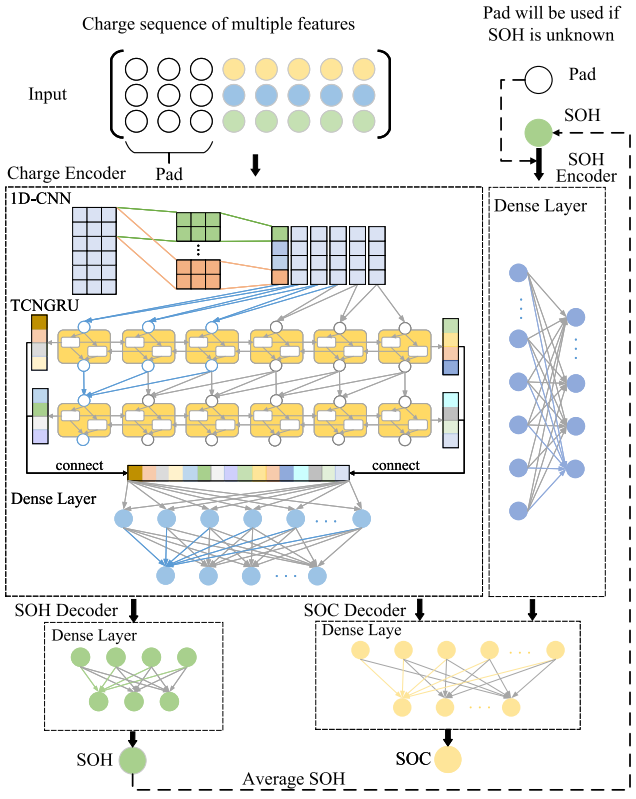


**Fig. 3.** Process of joint estimation based on SSEF.

this limitation, padding is introduced at the beginning of the charging data, as depicted in Fig. 2(right). This enables the model to accurately estimate SOC for the entire duration of the charging process.

Furthermore, SOH is unknown in the early stages of CC charging, as the model is not yet capable of estimation it. Therefore, padding is also applied to the early stages of the SOH input. It is worth highlighting that the SOH input during the early phase of charging has minimal impact on SOC estimation accuracy. Consequently, padding the SOH data in this phase does not significantly affect the precision of SOC estimation. This assertion has been empirically verified through subsequent experimental procedures.

### 3.4. Online estimation

As shown in Fig. 3, the charge sequence of multiple features and the current SOH are encoded separately using the Charge encoder and SOH encoder. Subsequently, the SOC and SOH are estimated using the SOC decoder and SOH decoder, respectively. In the early stage of each charging cycle, when the length of the charge sequence is less than the model's input sequence length, padding is applied to the sequence. Also, when specific voltage fluctuations are not observed, accurate prediction of SOH is not feasible. In this case, only SOC is estimated, and the SOH part of the model input is padded. As charging progresses and the voltage enters a specific range, the model can estimate both SOC and SOH. To better represent the estimated value of SOH, the final result of SOH is the average of the estimated SOH values of known sequences.

## 4. Dataset description and experiment

### 4.1. Dataset description

The objective of this research is to explore a novel framework for the joint estimation of SOC and SOH using battery charging data.

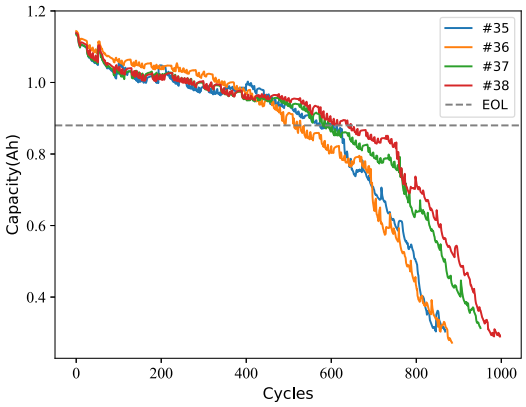


**Fig. 4.** Actual capacity change of different batteries.

Therefore, the selected dataset for testing should include both the capacity and charge variations throughout the whole-life-cycle charging process. The dataset used in this study was obtained from the University of Maryland. The data were collected through continuous charging–discharging experiments using the Arbin BT2000 battery experimental system at the Center for Advanced Life Cycle Engineering [37]. All CS2 cells followed the same charging profile, which consisted of a standard CC–CV protocol. The experiments were conducted at a controlled ambient temperature of 25 °C, utilizing the CC–CV charging protocol for battery charging. During the CC charging process, data is collected every 30 s.

Four batteries (#35, #36, #37 and #38) were selected from the dataset for this study. All batteries feature lithium cobalt oxide ($LiCoO_2$) as the positive electrode material, with a nominal capacity of 1.1Ah and a nominal voltage of 4.2 V. The dataset encompasses comprehensive information regarding the aging process, including voltage, current, charging time, and other relevant parameters, providing insights into the battery's degradation throughout its entire lifespan. For the subsequent experiments, #35, #36, and #38 were chosen as the training dataset, while #37 was selected as the test dataset to evaluate the performance of the training results.

The degradation curves of the four cell capacities are presented in Fig. 4, revealing three distinct characteristics. Firstly, the degradation process of the capacities exhibits significant variations among the different batteries. Secondly, the trend of capacity degradation is nonlinear, with an increasing degradation rate as the lifecycle progresses. Thirdly, the capacity degradation of the cells follows an oscillatory decline pattern rather than a monotonic decrease. In this study, the end of life (EOL) was defined as reaching 80% of the initial capacity. Subsequent data analysis primarily focuses on the lifespan within the designated timeframe.

Fig. 5 depicts a complete CC–CV charging process with an initial constant current of 0.55 A, transitioning to a constant voltage of 4.2 V once the voltage reaches 4.2 V. Fig. 6 shows the voltage and current profiles during the whole-life-cycle of CC–CV charging for the four batteries. The duration to reach the rated voltage decreases as the battery's lifecycle progresses during the constant current charging process, supporting the relationship between remaining capacity and constant current charging. The voltage range for CC charging mainly spans [3.5 V, 4.2 V], with the voltage initially rising rapidly and then transitioning to a gradual increase, and the ascent rate becoming more pronounced. Previous studies [35,38,39] have used parameter variations during charging to estimate SOH. In this referenced study [34], data capturing voltage variations within a specific range during the CC charging phase were employed for SOH estimation. After careful observation and experimentation, a voltage range of [3.7 V, 3.95 V] was chosen. Testing confirmed that utilizing data within this range yields accurate estimation of SOH.

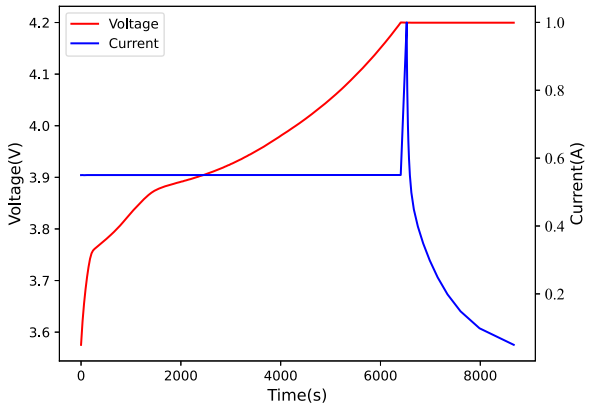


**Fig. 5.** Voltage and current curves of a CC–CV cycle.

Many studies [14,34,38] have already analyzed and validated that voltage, current, and time variations in battery data are the most appropriate input parameters for estimating SOC and SOH. Therefore, we will not delve further into these aspects. In this dataset, the data collection interval during the CC charging process is fixed. Here, the time parameter has limited impact on the model, and therefore, we choose to focus solely on voltage and current as the input parameters for our model.

### 4.2. Evaluation metrics

In order to evaluate the estimated performance of the model for SOH and SOC, three distinct evaluation metrics were utilized: Mean Absolute Error (MAE), Maximum Absolute Error (MAX), and RMSE. These metrics provide measures of the average error magnitude, identification of potential outliers or significant deviations, and comprehensive assessment of the model's accuracy by considering both the magnitude and direction of the estimation errors. MAE, MAX and RMSE are given as:

$$\mathrm{MAE} = \frac{1}{n}\sum_{i=1}^{n}\left|\hat{y}_i - y_i\right| \tag{9}$$

$$\mathrm{MAX} = \max_{i=1}^{n}\left|\hat{y}_i - y_i\right|_i \tag{10}$$

$$\mathrm{RMSE} = \sqrt{\frac{1}{n}\sum i = 1^{n}\left(\hat{y}_i - y_i\right)^2} \tag{11}$$

where $y_i$ represents the actual value, $\hat{y}_i$ represents the estimated value, and $n$ represents the number of test samples.

By employing these three evaluation metrics, a comprehensive evaluation of the proposed model's performance in estimating SOH and SOC is achieved, accounting for various aspects of estimation accuracy.

### 4.3. Experiment setup

The experimental procedure in this study comprises the following four steps:

1. Model Configuration: The Adam optimizer is employed for the entire model training process with a learning rate (lr) of 0.001. The maximum training epoch is set to 300. Batch size is set to 1024. The data sequence length is defined as 80, while the feature length for both the CNN and GRU layers is set to 128. The CNN layer adopts a convolution kernel size of 3.

2. Hyperparameter settings: $\alpha$ and $\beta$ represent two hyperparameters. We explored various values, including [0.5, 0.5], [0.7, 0.3], [0.9, 0.1], and ultimately opted for [0.3, 0.7]. At this configuration, we achieved a robust estimation of SOH, and simultaneously, the estimation of SOC showed favorable results.

3. Joint Estimation of SOH and SOC: The training is conducted using CC charging data within the voltage range of [3.7 V, 3.95 V] that covers the entire lifespan of the batteries. The joint encoder is designed to learn the sequence information related to both SOH and SOC simultaneously, resulting in the optimal model for SOH estimation.

4. SOC Estimation: The training for SOC estimation is performed using the CC charging data that spans the entire battery lifespan, along with the encoder obtained from the second step.

5. Testing: The trained model is utilized to perform joint estimation of SOC and SOH.

All implementations in this paper were conducted using Python 3.8 and TensorFlow 2.2.0. The experiments were performed on an Ubuntu 18.04 operating system, utilizing a 3090ti graphics card.

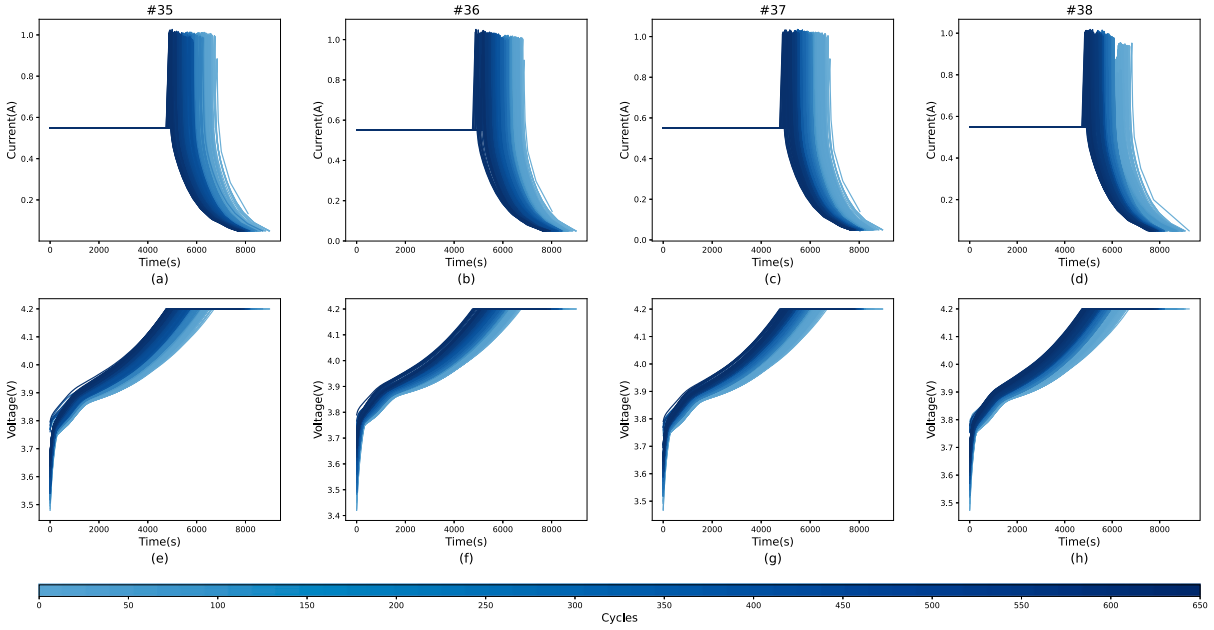


**Fig. 6.** Voltage and current curves for CC–CV charging over the whole-life-cycle. (a) and (e) are curves of #35. (b) and (f) are curves of #36. (c) and (g) are curves of #37. (d) and (h) are curves of #38.

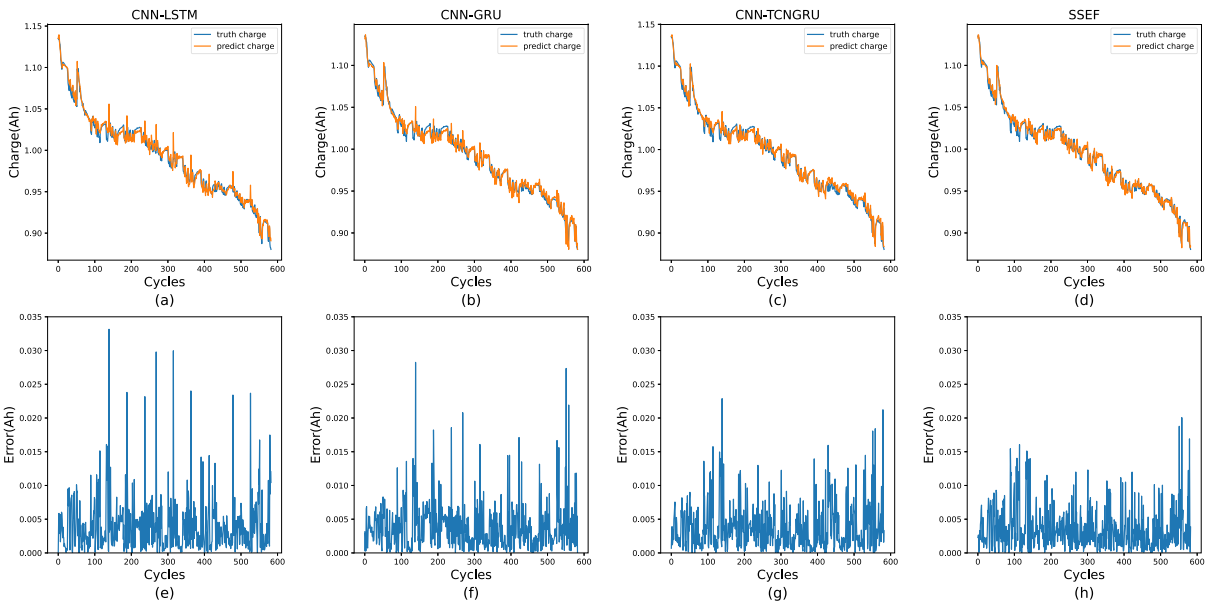


**Fig. 7.** SOH estimation results of different models. (a) and (e) are results of CNN–LSTM. (b) and (f) are results of CNN-GRU. (c) and (g) are results of CNN-TCNGRU. (d) and (h) are results of SSEF.

**Table 1**
Comparison of SOH and SOH-A estimation results.

| Model | SOH | | | SOH-A | | |
|---|---|---|---|---|---|---|
| | MAE | MAX | RMSE | MAE | MAX | RMSE |
| 1D-CNN [35] | 0.00555 | 0.06066 | 0.00738 | 0.00550 | 0.06066 | 0.00788 |
| SBLSTM [18] | 0.00512 | 0.03189 | 0.00655 | 0.00474 | 0.02847 | 0.00629 |
| TCN-LSTM [19] | 0.00636 | 0.04452 | 0.00830 | 0.00547 | 0.03618 | 0.00756 |
| CNN–LSTM [30] | 0.00442 | 0.03739 | 0.00593 | 0.00405 | 0.03315 | 0.00576 |
| CNN-GRU [33] | 0.00414 | 0.03441 | 0.00535 | 0.00386 | 0.02825 | 0.00535 |
| CNN-TCNGRU | **0.00400** | 0.02553 | **0.00521** | 0.00381 | 0.02287 | 0.00513 |
| SSEF | 0.00410 | **0.02177** | 0.00525 | **0.00358** | **0.02006** | **0.00479** |

### 4.4. Evaluation of SOH estimation performance

As mentioned earlier, #35, #36, and #38 were selected as the training dataset, while #37 was designated as the testing dataset. The CC charging data within the voltage range of [3.7 V, 3.95 V] was specifically chosen to estimate the joint model of SOC and SOH, allowing us to leverage more informative features through the joint encoding component and obtain separate models for SOH estimation.

In this experimental section, we compare the baseline models of 1D-CNN [35], SBLSTM [18], TCN-LSTM [19], CNN–LSTM [30], CNN-GRU [33], and CNN-TCNGRU for SOH estimation. And, these models adopt the same structure and parameter settings as the SOH component of SSEF, with the distinction lying in their respective core feature extraction components. Additionally, these models are single-objective models specifically designed for estimating SOH.

The experimental results, as shown in Table 1, demonstrate that SSEF achieves the best overall performance. Among CNN–LSTM and CNN-GRU, CNN-GRU performs exceptionally well. Therefore, GRU is selected as part of the encoding module in SSEF. The difference between these two models and others lies in the incorporation of the TCNGRU module. Here, we assert that the introduction of the TCNGRU module enhances the encoder's learning capabilities. This is mainly because the TCNGRU module possesses a more intricate model structure, thereby demonstrating stronger fitting capabilities to the data. Additionally, it is worth noting that within an acceptable range of errors, SSEF and CNN-TCNGRU demonstrate comparable performance in SOH estimation across key metrics such as MAE, MAX, and RMSE, outperforming the other three models. During the training process, only

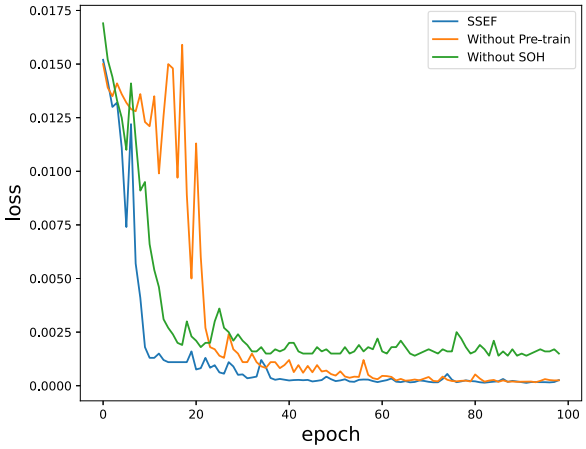


**Fig. 8.** Training loss for SOC estimation.

SOH is involved in training, while SOH-A is not directly engaged in training. However, when considering SOH-A, SSEF outperforms both CNN-TCNGRU and the other three models across all three metrics. This indicates that the joint estimation of SOH and SOC in SSEF enables the encoder to capture and leverage more feature information from the charging data, thus improving the estimation performance of SOH-A. This observation indirectly supports the conjecture of an inherent coupling between SOH and SOC.

To provide a more intuitive assessment of the estimation performance, Figures (a) and (e), (b) and (f), (c) and (g), (d) and (h) in Fig. 7 illustrate the SOH-A estimation results and corresponding errors of CNN–LSTM, CNN-GRU, CNN-TCNGRU and SSEF respectively. By examining the Error results displayed in these figures, we can gain insights into the performance of each model. The smaller the error, the closer the estimated values are to the ground truth, indicating a more accurate estimation of SOH. It is evident that SSEF consistently exhibits the best overall estimation performance, with error values consistently falling within a relatively small range.

Therefore, this comprehensive approach, as compared to the individual estimation of SOH in the other models, enables SSEF to achieve

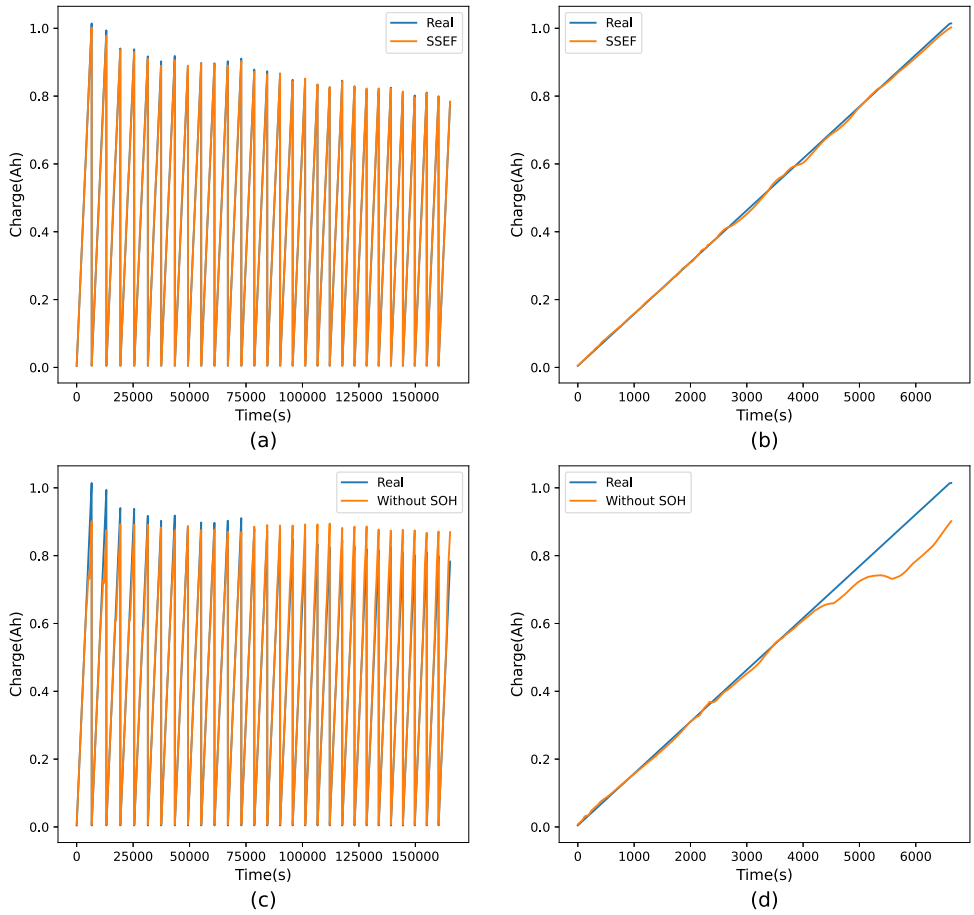


**Fig. 9.** SOC estimation results. (a) SOC estimation results of the SSEF model. (b) SSEF estimations for the first cycle. (c) Estimation results of the model Without SOH. (d) Estimations for the first cycle of the model Without SOH.

**Table 2**
Comparison of SOC estimation results among SSEF, Without Pre-train and Without SOH.

| Model | MAE | MAX | RMSE |
|---|---|---|---|
| SSEF | 0.00362 | 0.02136 | 0.00515 |
| Without Pre-train | 0.00438 | 0.03458 | 0.00624 |
| Without SOH | 0.01639 | 0.14078 | 0.02930 |

superior performance, as demonstrated by its lower error rates and more reliable estimations.

### 4.5. Evaluation of SOC estimation performance

The training of the SOC estimation model in SSEF involves leveraging the pretrained encoder component from the previous step and incorporating the current battery's actual capacity as an input. It is noteworthy that the parameters of the encoder component remain frozen, ensuring they are not subject to further training. To evaluate the effectiveness of SOC estimation in SSEF, a comparative analysis is conducted, contrasting the performance of the SSEF SOC estimation model with and without pretrained encoder component (Without Pre-train). Moreover, to further validate the efficacy of SSEF, an additional analysis is carried out by removing the input component that utilizes the actual capacity of the battery (Without SOH). Due to the high similarity among CC charging data from different cycles, we selected consecutive data from every 20 cycles for experimentation.

The variations in partial loss during the training process are depicted in Fig. 8, while the experimental results for different metrics are presented in Table 2. It is evident that SSEF outperforms the model structure without a pre-trained encoder on every metric, indicating the efficacy of pre-training the encoder in capturing SOH-related features and extracting more valuable information from the data. Furthermore, the training loss curve demonstrates that SSEF exhibits the fastest rate of loss reduction. This can be attributed to the fact that the encoder component does not require further training, resulting in a reduced number of trainable parameters and accelerated training speed.

Fig. 9(a) depicts the SOC estimation results of the SSEF model, while Fig. 9(b) showcases the SSEF estimations for the first cycle of the test data. On the other hand, Fig. 9(c) illustrates the estimations of the model Without SOH, and Fig. 9(d) demonstrates the estimations for the first cycle of the test data using the model Without SOH. A comparison between Fig. 9(a) and (c) reveals that Without SOH significantly underperforms SSEF throughout the entire battery lifecycle. This discrepancy can be attributed to the absence of the current battery's actual capacity as an input in the model Without SOH, resulting in similar estimation trends across different cycles. This highlights the crucial role of knowing the current battery capacity for accurate charge estimation over the whole-life-cycle. Furthermore, from Fig. 9(d), it is evident that when the actual battery capacity is unknown, deviations in charge current estimation mainly occur in the latter half. To mitigate this, the SSEF model, as shown in Fig. 9(b), employs padding with 0 values in the initial part, and once the SSEF model estimates the current actual capacity of the battery, it utilizes this information as an input without compromising the estimation performance.

## 5. Conclusion

This paper proposes a novel joint estimation framework, namely SSEF, which distinguishes itself from the traditional approach of using

**Table 3**
The advantages and disadvantages of SSEF.

| Proposed | Descriptions |
|---|---|
| Advantages | 1. It employs a segmented training approach, enabling a single encoder to simultaneously extract features related to SOC and SOH.<br>2. The unification of SOC and SOH predictions within a single model facilitates joint prediction.<br>3. The alternating design of TCN and GRU imparts robust learning capabilities to the model. |
| Disadvantages | 1. The simultaneous prediction of SOC and SOH is more complex compared to single-target models, making hyperparameter tuning more intricate.<br>2. The TCN-GRU approach is limited by GRU's sequential dependency, hindering full parallel computation akin to a pure convolutional model. |

two separate models for SOH and SOC estimations. SSEF leverages a single encoder and two decoders to simultaneously estimate SOH and SOC, significantly reducing model complexity and computational burden. We have designed a purpose-built encoder that comprises an alternating combination of TCN and BiGRU in its core feature extraction component. This encoder effectively captures the relevant feature information associated with SOH and SOC from the charging data. Additionally, we explore a stepwise training approach, initially training the encoder and SOH decoder using a dual-objective model, followed by targeted training of the SOC decoder. Through extensive experimentation, it has been demonstrated that the SSEF, utilizing the proposed encoder, exhibits superior performance in estimating SOH. This superiority is evident across key performance metrics, including MAE, MAX and RMSE. Subsequently, the advantages of the SSEF framework in SOC estimation were also demonstrated. The detailed comparison of SSEF's advantages and disadvantages is outlined in Table 3.

Although SSEF demonstrates promising performance in estimating both SOH and SOC, there are still some limitations to address. Compared to a single-target model, the simultaneous estimation model for SOC and SOH has a more complex structure. Additionally, the TCN-GRU computation efficiency is relatively lower compared to a pure convolutional structure, and the transferability of the decoder module across datasets requires further validation and optimization. Future research will focus on optimizing the model to address these issues.

## CRediT authorship contribution statement

**Haichi Huang:** Investigation, Conceptualization, Methodology, Formal analysis, Writing – original draft. **Chong Bian:** Data curation, Software, Writing – review & editing. **Mengdan Wu:** Validation, Formal analysis. **Dong An:** Supervision, Project administration, Funding acquisition, Writing – review & editing. **Shunkun Yang:** Supervision, Resources, Software, Project administration, Writing – review & editing.

## Declaration of competing interest

The authors declare that they have no known competing financial interests or personal relationships that could have appeared to influence the work reported in this paper.

## Data availability

I used a public data set and explained it in the corresponding section of the article.

## Acknowledgments

This research was supported by the National Key R&D Program of China [grant number 2022YFE0107100].

## References

[1] Zine Bachir, Marouani Khoudir, Becherif Mohamed, Yahmedi Said. Estimation of battery SOC for hybrid electric vehicle using coulomb counting method. Int J Emerg Electr Power Syst 2018;19(2):20170181.
[2] Tian Jinpeng, Xiong Rui, Shen Weixiang, Sun Fengchun. Electrode ageing estimation and open circuit voltage reconstruction for lithium ion batteries. Energy Storage Mater 2021;37:283–95.
[3] Lin Cheng, Tang Aihua, Xing Jilei. Evaluation of electrochemical models based battery state-of-charge estimation approaches for electric vehicles. Appl Energy 2017;207:394–404.
[4] Yang Fangfang, Xing Yinjiao, Wang Dong, Tsui Kwok-Leung. A comparative study of three model-based algorithms for estimating state-of-charge of lithium-ion batteries under a new combined dynamic loading profile. Appl Energy 2016;164:387–99.
[5] Galeotti Matteo, Cinà Lucio, Giammanco Corrado, Cordiner Stefano, Di Carlo Aldo. Performance analysis and SOH (state of health) evaluation of lithium polymer batteries through electrochemical impedance spectroscopy. Energy 2015;89:678–86.
[6] Zhang Wei, Ma Fenfen, Guo Sibei, Chen Xin, Zeng Ziqi, Wu Qiang, Li Shuping, Cheng Shijie, Xie Jia. A model cathode for mechanistic study of organosulfide electrochemistry in Li-organosulfide batteries. J Energy Chem 2022;66:440–7.
[7] Liu Yiwei, Sun Jing, Shang Yunlong, Zhang Xiaodong, Ren Song, Wang Diantao. A novel remaining useful life prediction method for lithium-ion battery based on long short-term memory network optimized by improved sparrow search algorithm. J Energy Storage 2023;61:106645.
[8] Farmann Alexander, Waag Wladislaw, Marongiu Andrea, Sauer Dirk Uwe. Critical review of on-board capacity estimation techniques for lithium-ion batteries in electric and hybrid electric vehicles. J Power Sources 2015;281:114–30.
[9] Lyu Zhiqiang, Gao Renjing, Chen Lin. Li-ion battery state of health estimation and remaining useful life prediction through a model-data-fusion method. IEEE Trans Power Electron 2020;36(6):6228–40.
[10] Ma L, Hu C, Cheng F. State of charge and state of energy estimation for lithium-ion batteries based on a long short-term memory neural network. J Energy Storage 2021;37:102440.
[11] Ma Yan, Shan Ce, Gao Jinwu, Chen Hong. A novel method for state of health estimation of lithium-ion batteries based on improved LSTM and health indicators extraction. Energy 2022;251:123973.
[12] Guo Shanshan, Ma Liang. A comparative study of different deep learning algorithms for lithium-ion batteries on state-of-charge estimation. Energy 2023;263:125872.
[13] Chemali Ephrem, Kollmeyer Phillip J, Preindl Matthias, Emadi Ali. State-of-charge estimation of li-ion batteries using deep neural networks: A machine learning approach. J Power Sources 2018;400:242–55.
[14] Zhao Ruxiu, Kollmeyer Phillip J, Lorenz Robert D, Jahns Thomas M. A compact methodology via a recurrent neural network for accurate equivalent circuit type modeling of lithium-ion batteries. IEEE Trans Ind Appl 2018;55(2):1922–31.
[15] Chen Junxiong, Feng Xiong, Jiang Lin, Zhu Qiao. State of charge estimation of lithium-ion battery using denoising autoencoder and gated recurrent unit recurrent neural network. Energy 2021;227:120451.
[16] Wang Ya-Xiong, Chen Zhenhang, Zhang Wei. Lithium-ion battery state-of-charge estimation for small target sample sets using the improved GRU-based transfer learning. Energy 2022;244:123178.
[17] Bian Chong, He Huoliang, Yang Shunkun, Huang Tingting. State-of-charge sequence estimation of lithium-ion battery based on bidirectional long short-term memory encoder-decoder architecture. J Power Sources 2020;449:227558.
[18] Bian Chong, He Huoliang, Yang Shunkun. Stacked bidirectional long short-term memory networks for state-of-charge estimation of lithium-ion batteries. Energy 2020;191:116538.
[19] Hu Chunsheng, Cheng Fangjuan, Ma Liang, Li Bohao. State of charge estimation for lithium-ion batteries based on TCN-LSTM neural networks. J Electrochem Soc 2022;169(3):030544.
[20] Deng Zhongwei, Yang Lin, Cai Yishan, Deng Hao, Sun Liu. Online available capacity prediction and state of charge estimation based on advanced data-driven algorithms for lithium iron phosphate battery. Energy 2016;112:469–80.
[21] Li Yi, Zou Changfu, Berecibar Maitane, Nanini-Maury Elise, Chan Jonathan C-W, Van den Bossche Peter, Van Mierlo Joeri, Omar Noshin. Random forest regression for online capacity estimation of lithium-ion batteries. Appl Energy 2018;232:197–210.
[22] Li Hong, Pan Donghui, Chen CL Philip. Intelligent prognostics for battery health monitoring using the mean entropy and relevance vector machine. IEEE Trans Syst Man Cybern: Syst 2014;44(7):851–62.

[23] Dong Guangzhong, Han Weiji, Wang Yujie. Dynamic Bayesian network-based lithium-ion battery health prognosis for electric vehicles. IEEE Trans Ind Electron 2020;68(11):10949–58.
[24] Urolagin Siddhaling, Sharma Nikhil, Datta Tapan Kumar. A combined architecture of multivariate LSTM with Mahalanobis and Z-Score transformations for oil price forecasting. Energy 2021;231:120963.
[25] Guo Ruohan, Shen Weixiang. A data-model fusion method for online state of power estimation of lithium-ion batteries at high discharge rate in electric vehicles. Energy 2022;254:124270.
[26] You Gae-Won, Park Sangdo, Oh Dukjin. Diagnosis of electric vehicle batteries using recurrent neural networks. IEEE Trans Ind Electron 2017;64(6):4885–93.
[27] Tan Yandan, Zhao Guangcai. Transfer learning with long short-term memory network for state-of-health prediction of lithium-ion batteries. IEEE Trans Ind Electron 2019;67(10):8723–31.
[28] Li Penghua, Zhang Zijian, Xiong Qingyu, Ding Baocang, Hou Jie, Luo Dechao, Rong Yujun, Li Shuaiyong. State-of-health estimation and remaining useful life prediction for the lithium-ion battery based on a variant long short term memory neural network. J Power Sources 2020;459:228069.
[29] Li Penghua, Zhang Zijian, Grosu Radu, Deng Zhongwei, Hou Jie, Rong Yujun, Wu Rui. An end-to-end neural network framework for state-of-health estimation and remaining useful life prediction of electric vehicle lithium batteries. Renew Sustain Energy Rev 2022;156:111843.
[30] Xu Huanwei, Wu Lingfeng, Xiong Shizhe, Li Wei, Garg Akhil, Gao Liang. An improved CNN-LSTM model-based state-of-health estimation approach for lithium-ion batteries. Energy 2023;276:127585.
[31] Han Te, Wang Zhe, Meng Huixing. End-to-end capacity estimation of lithium-ion batteries with an enhanced long short-term memory network considering domain adaptation. J Power Sources 2022;520:230823.
[32] Yang Duo, Zhang Xu, Pan Rui, Wang Yujie, Chen Zonghai. A novel Gaussian process regression model for state-of-health estimation of lithium-ion battery using charging curve. J Power Sources 2018;384:387–95.
[33] Zheng Yuxuan, Hu Jiaxiang, Chen Jianjun, Deng Huiwen, Hu Weihao. State of health estimation for lithium battery random charging process based on CNN-GRU method. Energy Rep 2023;9:1–10.
[34] Deng Zhongwei, Hu Xiaosong, Li Penghua, Lin Xianke, Bian Xiaolei. Data-driven battery state of health estimation based on random partial charging data. IEEE Trans Power Electron 2021;37(5):5021–31.
[35] Qian Cheng, Xu Binghui, Chang Liang, Sun Bo, Feng Qiang, Yang Dezhen, Ren Yi, Wang Zili. Convolutional neural network based capacity estimation using random segments of the charging curves for lithium-ion batteries. Energy 2021;227:120333.
[36] Li Yihuan, Li Kang, Liu Xuan, Li Xiang, Zhang Li, Rente Bruno, Sun Tong, Grattan Kenneth TV. A hybrid machine learning framework for joint SOC and SOH estimation of lithium-ion batteries assisted with fiber sensor measurements. Appl Energy 2022;325:119787.
[37] He Wei, Williard Nicholas, Osterman Michael, Pecht Michael. Prognostics of lithium-ion batteries based on Dempster–Shafer theory and the Bayesian Monte Carlo method. J Power Sources 2011;196(23):10314–21.
[38] Shen Sheng, Sadoughi Mohammadkazem, Li Meng, Wang Zhengdao, Hu Chao. Deep convolutional neural networks with ensemble learning and transfer learning for capacity estimation of lithium-ion batteries. Appl Energy 2020;260:114296.
[39] Tian Jinpeng, Xiong Rui, Shen Weixiang, Lu Jiahuan, Yang Xiao-Guang. Deep neural network battery charging curve prediction using 30 points collected in 10 min. Joule 2021;5(6):1521–34.